ACS OMEGA

http://pubs.acs.org/journal/acsodf

Article

Effect of Acetylene Links on Electronic and Optical Properties of Semiconducting Graphynes

Yang Li,[‖] Junhan Wu,[‖] Chunmei Li, Qiang Wang,* and Lei Shen*

Cite This: *ACS Omega* 2021, 6, 10997−11004

Read Online

ACCESS | Metrics & More | Article Recommendations | Supporting Information

ABSTRACT: The family of graphynes, novel two-dimensional semiconductors with various and fascinating chemical and physical properties, has attracted great interest from both scientific and industrial communities. Currently, the focus is on graphdiyne or graphyne-2. In this work, we systematically study the effect of acetylene, i.e., carbon−carbon triple bond, links on the electronic and optical properties of a series of graphynes (graphyne-*n*, where *n* = 1−5, the number of acetylene bonds) using ab initio calculations. We find an even−odd pattern, i.e., *n* = 1, 3, 5 and *n* = 2, 4 having different features, which has not been discovered in studying graphyne or graphdiyne alone. It is found that as the number of acetylene bonds increases, the electron effective mass increases continuously in the low-energy range because of the flatter conduction band induced by the longer acetylene links. Meanwhile, longer acetylene links result in a larger red shift of the imaginary part of the dielectric function, loss function, and extinction coefficient. In this work, we propose an effective method to tune and manipulate both the electronic and optical properties of graphynes for the applications in optoelectronic devices and photochemical catalysis.

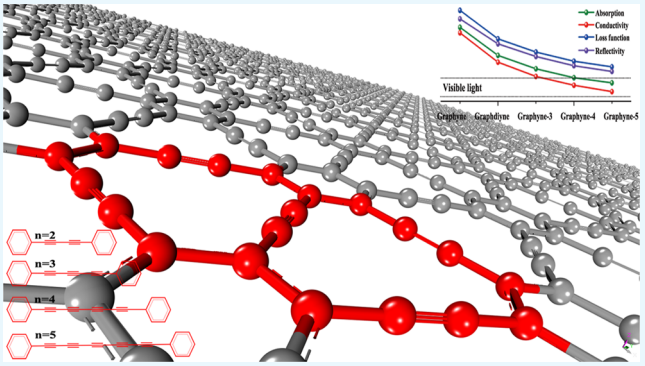

1. INTRODUCTION

The large variety of carbon allotropes, showing different physical and chemical properties, is due to the different carbon hybridizations, i.e., sp, sp^2, and sp^3. For example, the natural three-dimensional (3D) graphite and diamond are formed through sp^2 and sp^3 hybridizations of carbon atoms, respectively. Meanwhile, the sp^2 hybridization occurs in some novel man-made carbon allotropes, such as fullerene,[1] carbon nanotube,[2] and graphene.[3] In 1987, the concept of sp−sp^2 hybridized graphyne-*n* was theoretically proposed by Baughman,[4] where *n* indicated the number of carbon−carbon triple (acetylene) bonds in graphyne (see Figure 1). Accordingly, there are several kinds of structures based on the polymerization mode, such as graphyne (*n* = 1), graphdiyne (*n* = 2), graphyne-3 (*n* = 3), and so on. After the successful synthesis of graphyne (*n* = 1) in the experiment, it has been of particular interest due to its unique semiconducting electronic structure and extensive applications in many fields, such as catalysis, sensor and transistor technologies, and energy storage (see reviews[5,6] and references therein). Simultaneously, engineering of tuning the electronic structure by simply constructing the acetylene bonds *n* has been attracted more and more attention to this kind of two-dimensional (2D) materials theoretically and experimentally.

Recently, 2D semiconducting graphyne-2 has been synthesized on a copper surface by the cross-coupling reaction.[7−9] Soon, these types of 2D materials attracted great attention in many research fields, such as catalysis, energy storage, water purification, and optoelectronic devices, due to their large interlayer distance, unique porous structure, large specific surface area, and high conductivity.[10−19] Theoretical calculations reveal that graphyne-2 has higher electron mobility than graphene.[20,21] Kuang et al.[22] further pointed out that the electron mobility and photoconversion efficiency of perovskite solar cells with doped graphyne-2 were significantly improved, which paves the way for optoelectronic applications of graphyne-2. Wang et al.[17] synthesized graphyne-2 composites by the hydrothermal method, which exhibited excellent photocatalytic degradation of methylene blue. The π-conjugated structure in graphyne-2 makes it efficient to receive photogenerated electrons in the conduction band and to suppress the recombination of electrons and holes. Luo et al.[23] found that the multibody effect had a significant impact on the electronic structure and optical absorption of graphyne-2 both theoretically and experimentally. Due to the additional acetylene bond in graphyne-2 compared with graphyne-1, graphyne-2 has a larger porous and much softer structure than graphyne-1, which

Received: February 16, 2021
Accepted: April 6, 2021
Published: April 19, 2021

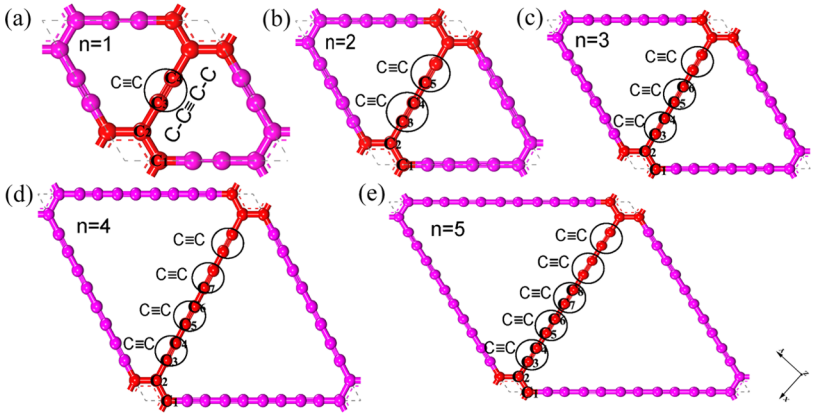

Figure 1. Optimized geometric structures of unit cells of 2D graphynes. Each graphyne is named with an index "*n*", which indicates the number of carbon−carbon triple bonds in a link, highlighted in red, between two adjacent hexagons: (a) graphyne-1, (b) graphyne-2, (c) graphyne-3, (d) graphyne-4, and (e) graphyne-5.

Table 1. Lattice Constants and Cohesive Energies of Graphynes

		graphyne	graphdiyne	graphyne-3	graphyne-4	graphyne-5
lattice constant (Å)	this work	6.872	9.436	12.011	14.576	17.592
	other works	6.86[a], 6.877[b], 6.89[c]	9.44[a], 9.46[c], 9.490[c]	12.02[a], 12.04[c], 12.43[d]	14.6[a], 14.60[c]	
cohesive energy (eV atom^{-1})	this work	8.635	8.513	8.450	8.419	8.397
	other works	7.95[a], 7.21[e]	7.78[a], 7.87[e]	7.70[a]	7.66[a]	

[a]Ref 31. [b]Ref 32. [c]Ref 33. [d]Ref 34. [e]Ref 29.

indicates that graphdiyne could easily form a hybrid with other materials for optical applications.[5,6] The difference in the electronic structures and mechanical properties between graphyne and graphdiyne as well as the resulting different potential applications has accelerated the engineering and application of the graphyne-*n* family, especially in the properties of graphyne-*n* with longer acetylene links beyond $n = 1$ and 2.

In this paper, the electronic and optical properties of five members in the graphyne family, i.e., graphyne-*n* ($n = 1-5$), are systemically investigated using ab initio calculations. It was found that the length of the acetylene links greatly changes the feature of the energy bands near the Fermi level. Thus, both the electronic and optical properties of these types of 2D materials could be feasibly tuned and manipulated for optoelectronic devices and photochemical catalysis applications. This may open a way for exploring the extended graphynes in optoelectronic applications.

2. COMPUTATIONAL METHODS

In this work, we carried out ab initio calculations with the CASTEP module,[24] which was implemented in the framework of density functional theory (DFT)[25] using the generalized gradient approximation (GGA) in the parameterization of the Perdew−Burke−Ernzerhof (PBE) format exchange−correlation functional.[26] The Grimme[27] under dispersion correction (DFT-D) was used to improve the calculation accuracy of the weak interaction in 2D graphynes. The electron−ion interactions were described by the Vanderbilt ultrasoft pseudopotentials (US-PP).[26] The convergence test and geometric optimization of the graphyne-*n* unit cell were performed first. The kinetic cutoff energy used for plane wave expansions was 650 eV. For graphyne-1, graphyne-2, and graphyne-3, the Monkhorst−Pack *K*-point meshes of $11 \times 11 \times 1$ were used in the first Brillouin zone,[28] while for graphyne-4 and graphyne-5 with large unit cells, the Brillouin zone integrations were performed using a Monkhorst−Pack grid of $8 \times 8 \times 1$. The vacuum layer thickness was set to 15 Å to eliminate the interlayer interaction. Each calculation was converged when the total energy changes during the geometry optimization process were less than 1×10^{-5} eV/atom, and the force per atom and the residual stress of the unit cell were less than 0.01 eV/Å and 0.05 GPa, respectively. The maximum displacement between cycles was less than 0.005 Å when the convergence reached.

3. RESULTS AND DISCUSSION

3.1. Geometric Structures. The geometric structures of the unit cells of graphyne-1, graphyne-2, graphyne-3, graphyne-4, and graphyne-5 are shown in Figure 1. The size of the cavity of graphynes is proportional to the length of the acetylene linkages. The structural stability of graphynes can be estimated by the cohesive energy, which can be defined as follows.[29]

$$E_{coh} = \frac{n \times E_{atom} - E_{tot}}{n} \quad (1)$$

where E_{coh} is the cohesive energy of graphynes, n is the number of carbon atoms in a unit cell, and E_{atom} and E_{total} are the energy of a single carbon atom and the total energy in a unit cell, respectively. The details of the lattice constant, cohesive energy, and comparison with other reports are shown in Table 1. As can be seen, the calculated lattice parameters in this work are in good agreement with previously reported works. Our cohesive energies are slightly higher than other results, which might be due to the different pseudopotentials used.

It is noted that the cohesive energy is the energy required for separating the neutral atoms in the ground state at 0 K.[30] Thus, the larger the E_{coh}, the more stable the crystal structure. According to the calculated cohesive energies in Table 1, it can be found that the planar two-dimensional structure of graphyne-1 is the most stable. Meanwhile, the cohesive energy of

https://doi.org/10.1021/acsomega.1c00840
ACS Omega 2021, 6, 10997−11004

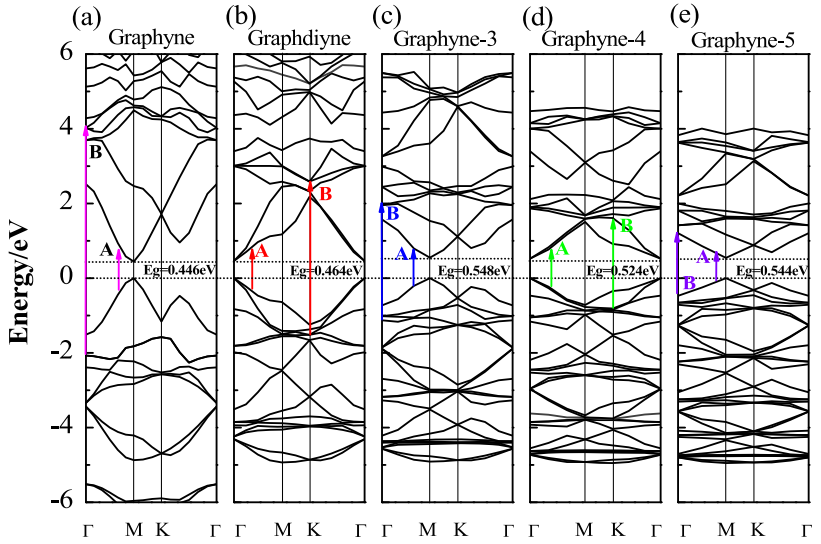

Figure 2. Energy-band structures of graphyne-*n*. E_g is the direct band gap. A and B indicate the possible electron excitation, hopping from the valence band to the conduction band.

Table 2. Values of the Effective Mass of Graphynes in the Conduction (m_c) and Valence Band (m_v) and the Band Gap (E_g)

	m_c/m_0		m_v/m_0		
structure	$\Gamma \rightarrow M$	$M \leftarrow K$	$\Gamma \rightarrow M$	$M \leftarrow K$	E_g (eV)
graphyne-1	0.146(0.15[a], 0.21[b])	0.086(0.063[a], 0.087[b])	0.150(0.17[a], 0.22[b])	0.068(0.066[a], 0.0901[b])	0.446 at M (0.46[c],0.47[d,e])
graphyne-2	0.080(0.073[a])		0.074(0.075)		0.464 at Γ (0.48,0.46[f,])
graphyne-3	0.082(0.099[a])	0.053(0.081[a])	0.106(0.12[a])	0.081(0.085[a])	0.548 at M (0.56[d])
graphyne-4	0.078(0.081[a])		0.110(0.080)		0.524 at Γ (0.54[d])
graphyne-5	0.101	0.091	0.133	0.120	0.544 at M

[a]Ref 31. [b]Ref 32. [c]Ref 33. [d]Ref 36. [e]Ref 37. [f]Ref 38. [g]Ref 39.

graphynes decreases gradually with the increase of the number of acetylene bonds (n).

3.2. Electronic Properties. Figure 2 shows the band structures of graphynes. It can be seen that all of them are direct-band-gap (E_g) semiconductors with band gaps of 0.446, 0.464, 0.548, 0.524, and 0.544 eV. It is worth noting that the band gap size is not simply linearly proportional to the number of acetylene bonds (n). Interestingly, the direct band gap of graphyne-*n* with odd *n*, i.e., n = 1, 3, 5, is located at the *M*-point, while it is at the Γ-point for even *n*. Meanwhile, the energy-band dispersions at the bottom of the conduction band and at the top of the valence band are quite similar for all graphynes, which indicates that they have similar effective mass of both electrons and holes.

The effective mass of electrons and holes in semiconductors is an essential parameter, which greatly affects the performance of electronic and/or optical devices. The effective mass of graphynes is calculated by the following equation.[35]

$$\frac{1}{m^*} = \frac{1}{\hbar^2}\frac{\partial^2 E(k)}{\partial k^2} \quad (2)$$

The values of the effective mass in the conduction band (m_c, holes) and valence band (m_v, electrons) are listed in Table 2. It is found that the effective mass is isotropic from *M* to *K* and Γ for graphyne-*n* with even (n = 2, 4) acetylene bonds, while it is anisotropic if *n* is odd. Our calculations show that the low energy levels of the conduction band are mainly contributed by the 2p state of carbon atoms, where the electrons have quite a small effective mass under the excitation of photons. This indicates that it facilitates the formation of the effective photogenerated electrons and the transferred charge carriers, while more effective photogenerated holes would be formed in the valence-band region.

It is found that all graphynes have covalent bonds from the Mulliken population (MP) analysis (Table S1), implying their good structural stability. Moreover, the MP analysis shows that the electronic states of graphynes are mainly contributed by the C-2p state, which is consistent with the projected density of state (PDOS) analysis shown in Figure S1. The bond lengths and band populations of C_1-C_2 (sp^2-sp^2), C_2-C_3 (sp^2-sp), C_4-C_5 ($sp-sp$), and C_6-C_7 ($sp-sp$) bonds of graphynes (see Figure 1) remain constant with the increase of the number of acetylene bonds (n). However, the bond lengths (band populations) of C_3-C_4, C_5-C_6, and C_7-C_8 ($sp\equiv sp$) bonds (Figure 1) are enlarged as *n* increases. These alternate bonding characteristics are also illustrated by the charge-density-difference calculations as shown in Figure S2. Such an alternate $-C\equiv C-C\equiv C-$ structure can energetically stabilize atomic carbon chains or rings, which have been reported in many carbon allotropes.[40,41]

3.3. Optical Properties. The calculated band structures of graphynes in Figure 2 show that they all are direct-band-gap semiconductors, and the values of band gaps are close to those of silicon (0.57 eV GGA-PBE[42]). Thus, we next study the optical properties of graphynes and their potential optoelectronic applications. It is well-known that standard GGA functionals like PBE underestimate the band gap. One of the major improvements in the band gap calculation is to use the hybrid functionals, such as HSE06.[43] However, both GGA-PBE and HSE06 give similar spectra except for an energy shift of

https://doi.org/10.1021/acsomega.1c00840
ACS Omega 2021, 6, 10997−11004

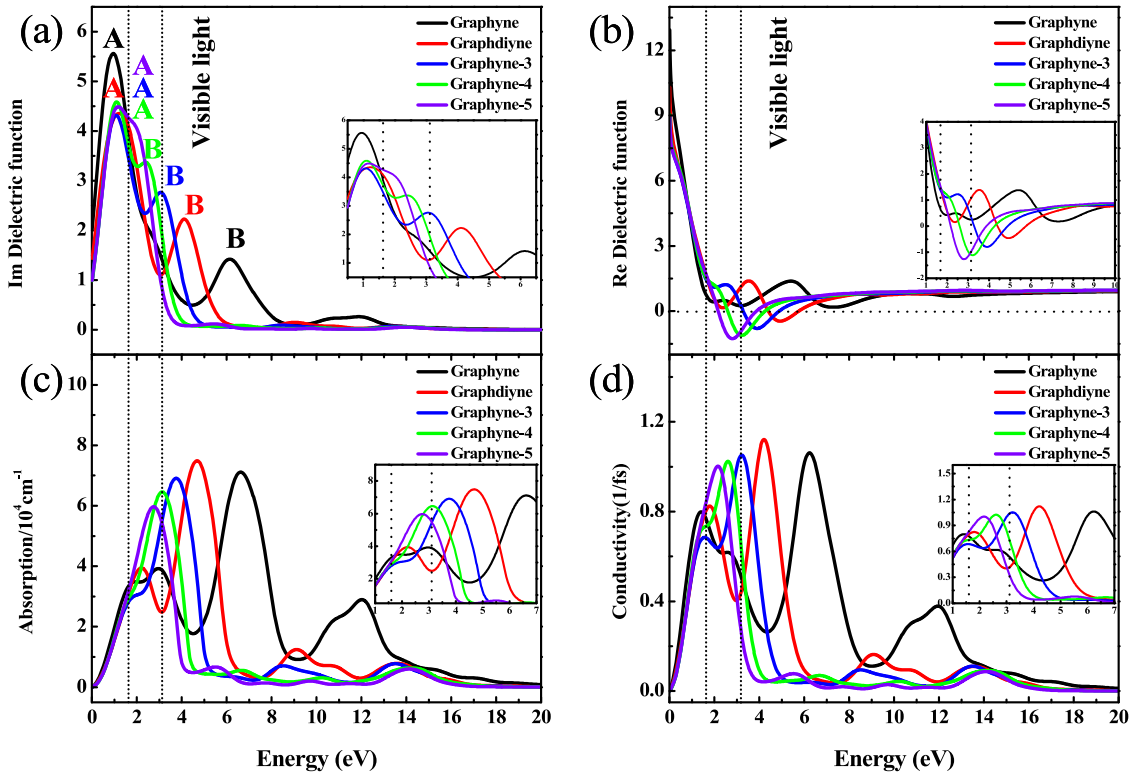

Figure 3. (a) Imaginary and (b) real parts of complex dielectric functions of graphynes. (c) Absorption function and (d) electrical conductivity of graphynes. The visible light region is labeled by two vertical dotted lines. The low-energy part is enlarged in the insets.

graphynes,[44] so only GGA-PBE results are presented in this work.

The complex dielectric function $\varepsilon(\omega)$, a significant parameter to determine the polarization effect inside materials, is calculated as

$$\varepsilon(\omega) = \varepsilon_1(\omega) + i\varepsilon_2(\omega) \tag{3}$$

where the imaginary part of the dielectric function $\varepsilon_2(\omega)$ describes the absorption of light and the real part of the dielectric function $\varepsilon_1(\omega)$ represents the amplitude modulation, that is, the resonant absorption of the electron transition.[45]

$$\varepsilon_1(\omega) = 1 + \frac{8\pi^2 e^2}{m^2} \cdot \sum_{V,C} \int_{BZ} d^3k \frac{2}{2\pi} \frac{|e \cdot M_{CV}(K)|^2}{[E_C(K) - E_V(K)]} \times \frac{\hbar^3}{[E_C(K) - E_V(K)]^2 - \hbar^2\omega^2} \tag{4}$$

$$\varepsilon_2(\omega) = \frac{4\pi^2}{m^2\omega^2} \cdot \sum_{V,C} \int_{BZ} d^3k \frac{2}{2\pi} |e \cdot M_{ev}(k)|^2 \times \delta[E_C(K) - E_V(K) - \hbar\omega] \tag{5}$$

$$I(\omega) = \sqrt{2}\,\omega[\sqrt{\varepsilon_1(\omega)^2 - \varepsilon_2(\omega)^2}\,]^{1/2} \tag{6}$$

$$\sigma(\omega) = \frac{\omega}{4\pi}\varepsilon_2(\omega) + i\left[\frac{\omega}{4\pi} - \frac{\omega}{4\pi}\varepsilon_1(\omega)\right] \tag{7}$$

$$n(\omega) = \frac{(n-1)^2 - k^2}{(n+1)^2 + k^2} \tag{8}$$

$$(\omega) = \frac{\varepsilon_2(\omega)}{\varepsilon_1(\omega)^2 + \varepsilon_2(\omega)^2} \tag{9}$$

$$R(\omega) = \left|\frac{\sqrt{\omega} - 1}{\sqrt{\omega} + 1}\right|^2 \tag{10}$$

where m is the free electron mass, e is the free electric charge, ω is the incident photon frequency, BZ is the first Brillouin zone, $|e \cdot M_{CV}(K)|$ is the momentum transition matrix element, K is the inverted lattice vector, k is the extinction coefficient, C is the conduction band, V is the valence band, and $E_C(K)$ and $E_V(K)$ are the intrinsic levels of the conduction and valence bands. Meanwhile, the absorption coefficient $I(\omega)$, conductivity $\sigma(\omega)$, refractive index $n(\omega)$, loss function $L(\omega)$, and reflectivity $R(\omega)$ can all be deduced from $\varepsilon(\omega)$ with the Kramers−Kronig dispersion.[46−48]

Figure 3 shows the calculated imaginary and real parts of the complex dielectric function, absorption function, and electrical conductivity of graphynes. The peak position of $\varepsilon_2(\omega)$ is determined by the band gap and the degree of nonlocalization in the low-energy regions. With the increase of the number of acetylene bonds, $\varepsilon_2(\omega)$ of graphynes has red-shifted as shown in Figure 3a. For the real part of the dielectric function $\varepsilon_1(\omega)$, the static dielectric constant (capacitance) is denoted $\varepsilon_1(0)$ at the zero frequency. The $\varepsilon_1(0)$ of graphynes is strongly dependent on the corresponding band gaps as shown in Table 3. Our results in Figure 3b show that $\varepsilon_1(\omega)$ dramatically decays to zero with the increase of the photon energies, indicating a resonance of the energy transition between electrons and photons in graphynes. Figure 3b shows that $\varepsilon_1(\omega)$ of graphyne-2−5 has negative values (positive for graphyne-1). According to the wave vector equation below

https://doi.org/10.1021/acsomega.1c00840
ACS Omega 2021, 6, 10997−11004

Table 3. Energy Corresponding to the Peak of the Imaginary Part of the Dielectric Function $\varepsilon_2(\omega)$, Energy of Electron Interband Transition, Static Dielectric Constant $\varepsilon_1(0)$, and Absorption Edges E_{op} of Graphynes

structure	photon energy (eV)	transition (eV)	ε_1 (0)	E_{op} (eV)
graphyne	A = 0.9	−0.20 → 0.70	12.9	5.37
	B = 6.1	−2.07 → 4.03		
graphdiyne	A = 1.2	−0.36 → 0.84	10.3	3.57
	B = 4.1	−2.64 → 1.46		
graphyne-3	A = 1.0	−0.21 → 0.79	8.9	2.65
	B = 3.0	−1.10 → 1.90		
graphyne-4	A = 1.1	−0.27 → 0.84	9.6	2.15
	B = 2.4	−0.80 → 1.60		
graphyne-5	A = 1.1	−0.25 → 0.85	8.9	1.79

$$\omega^2\varepsilon_1 = c^2(\mathbf{K}\cdot\mathbf{K}) \tag{11}$$

$\varepsilon_1 < 0$ means that the wave vector **K** is an imaginary number. Furthermore, this negative value region is red-shifted with the increase of the number of acetylene bonds (n) as shown in Figure 3b.

Figure 3c shows that the absorption coefficient in graphynes increases first and consequently decreases as the photon energy goes up. The peak of the absorption coefficient of graphynes shifts to the low-energy region and induces a narrow absorption range. Further analysis on the absorption function of graphyne-1 (Figure 3c) shows that there are four main absorption peaks at 1.95, 2.96, 6.63, and 12.03 eV, which are well consistent with the experimental values.[23] For graphyne-2 and graphyne-3, the highest peak is located within the ultraviolet region. Thus, they probably may have applications in ultraviolet protection or detection materials. The shift of the photoconductivity of graphynes with the photon energy is shown in Figure 3d. The conductivity peaks of graphyne-1 are at 1.46, 2.59, 6.24, and 11.97 eV. The profiles of the photoconductivity of graphynes shift to the low-energy region (Figure 3d), which approaches the energy range of the visible light.

The peak energy of the dielectric function $\varepsilon_2(\omega)$, energy of electron interband transition, static dielectric constant $\varepsilon_1(0)$, and absorption edges are presented in Table 3. For graphyne-1, the primary peaks of $\varepsilon_2(\omega)$ are located at A (0.9 eV) and B (6.1 eV). Based on the band structure in Figure 2, peak A mainly originates due to the transition between the unoccupied states at 0.70 eV and the occupied states at −0.20 eV. Meanwhile, peak B primarily originates from the transition from −2.07 to 4.03 eV of the 2p electrons in the valence band of the C atoms. The details of transitions of two peaks in $\varepsilon_2(\omega)$ of graphyne-2, graphyne-3, and graphyne-4 are summarized in Table 3. For graphyne-5, it is worth noting that the imaginary part of the dielectric function $\varepsilon_2(\omega)$ gives rise to a bimodal pattern, which shows only one peak at 1.1 eV due to the band localization and red shift of the functional profile (see in Figure 3). Furthermore, the transition between the occupied state at −0.25 eV and the empty state at 0.85 eV corresponds to peak A. Note that the peak in the imaginary part of the dielectric function $\varepsilon_2(\omega)$ may not correspond to a single interband transition (Figure 2), and other interband transitions at the same peak energy may also possibly occur in the band structure.[49,50]

The optical absorption edges of graphynes are shown in Figure 4. The optical absorption band edge E_{op} is described by the following extrapolation relationship[51]

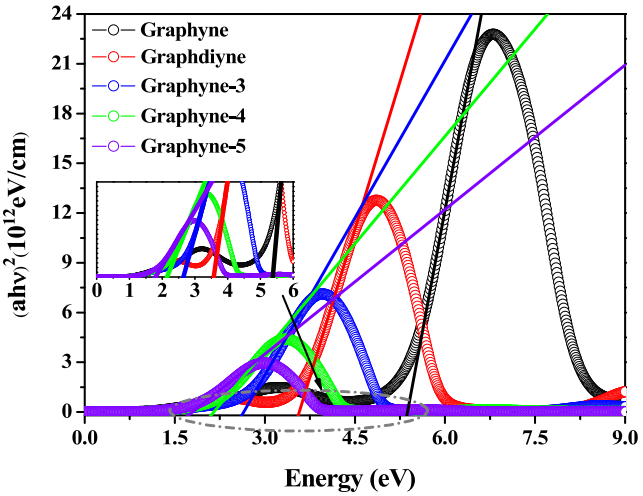

Figure 4. Optical absorption edges of graphynes, with the enlarged view shown in the inset.

$$\alpha h\nu = A(h\nu - E_{op})^n \tag{12}$$

where α represents the absorption spectrum, $h\nu$ is the photon energy, and A is a function of the refractive index of the material, the reduced mass, and the speed of light in vacuum. For direct-band-gap semiconductors, n takes 0.5.

The calculated values of the optical absorption band edge in graphyne-n are listed in Table 3. It is found that the absorption band edge shifts to the low-energy region with the increase of n. Moreover, there is a deviation between the absorption band edge and the corresponding band gap. It is mainly due to the electron localization in the free energy level of band structures.

The relationship between the complex refractive index $n(\omega)$ and extinction coefficient $k(\omega)$ with the photon energy of graphynes is shown in Figure 5a,b. At a frequency of zero, the static refractive indices of graphyne-n (n = 1−5) are located at 3.61, 3.22, 3.00, 3.01, and 2.99 eV, respectively. This indicates that the static index of refraction strongly depends on the band gap of graphynes. Furthermore, the complex refractive index of graphynes goes down first and then increases with an increase of the photon energy. The graphynes have distinct peaks of the energy loss in the calculated profile, as shown in Figure 5c. They correspond to the region of $\varepsilon_1(\omega) = 0$ and $\varepsilon_2(\omega) < 0$, which are the resonance peaks of the energy loss function in graphynes. The reflection spectrum of graphynes is shown in Figure 5d. Our results show that the reflectivity $R(0)$ of graphyne-1 approaches 32.2 and diminishes with the increase of the photon energy. The maximum value is 12.4% at a photon energy of 7.20 eV. Furthermore, as the acetylene bonds (n) increase, the profiles of the energy loss function shift to the low-energy region, and the electron localization and maximum values are enhanced (Figure S3).

CONCLUSIONS

In summary, we carried out ab initio studies on the geometric, electronic, and optical properties of 2D graphyne-n sheets, a family of sp−sp^2 hybrid materials with acetylene bonds. The odd−even pattern of n of graphynes on the position of direct band gaps and the dispersion of the effective mass are revealed by the electronic-structure calculation. Our photoelectron transport results show a red shift of the imaginary part of the dielectric function with the increase of the number of acetylene bonds. Furthermore, the loss function and extinction coefficient

https://doi.org/10.1021/acsomega.1c00840
ACS Omega 2021, 6, 10997−11004

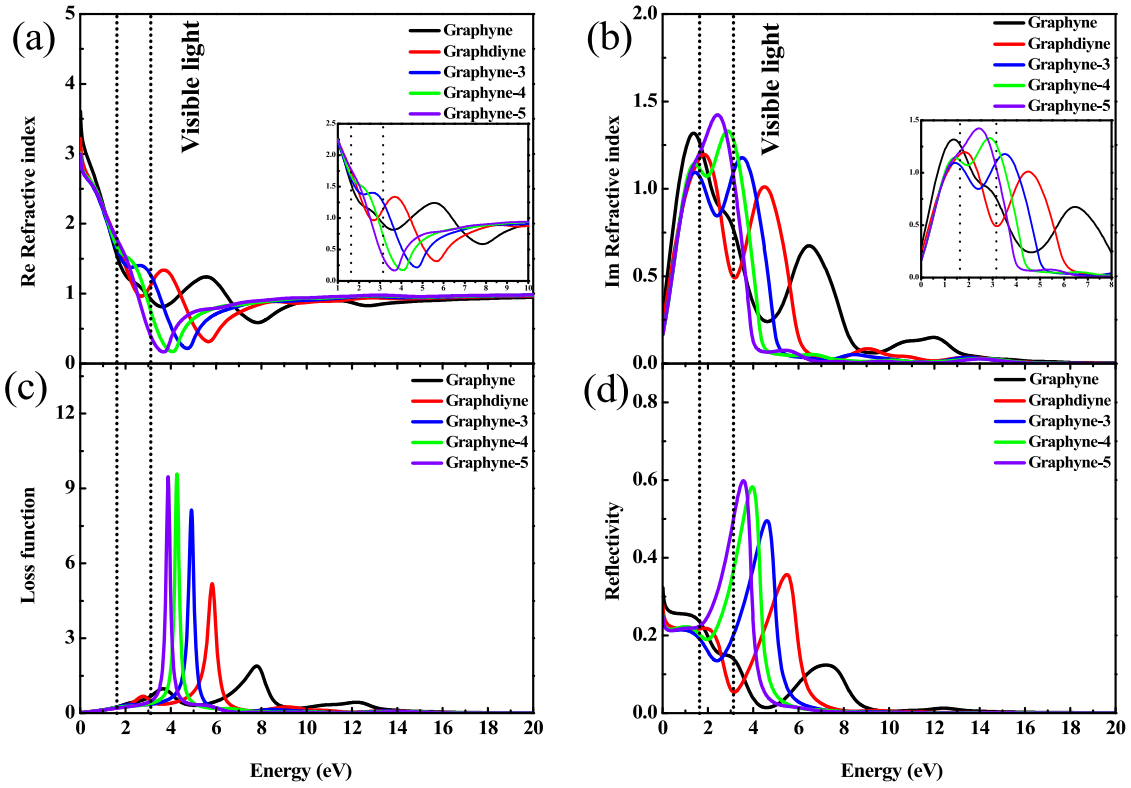

Figure 5. (a) Real and (b) imaginary parts of the complex refractive index of graphynes. (c) Loss function and (d) reflectivity of graphynes. The visible light region is labeled by two vertical dotted lines. The low-energy part is enlarged in the insets of (a) and (b).

move to the low-energy region with the increase of *n*. These findings show that the optical parameters could be tuned and manipulated by the number of acetylene bonds to fulfill different applications.

■ ASSOCIATED CONTENT

Supporting Information

The Supporting Information is available free of charge at https://pubs.acs.org/doi/10.1021/acsomega.1c00840.

Total and partial density of states, chemical bond analysis, charge density difference, and photoabsorption of graphyne-*n* (PDF)

■ AUTHOR INFORMATION

Corresponding Authors

Qiang Wang − *School of Materials and Energy, Southwest University, Chongqing 400715, China; Chongqing Key Laboratory for Advanced Materials and Technologies of Clean Energies, Southwest University, Chongqing 400715, P. R. China;* orcid.org/0000-0002-7396-0323; Email: wysnu@swu.edu.cn

Lei Shen − *Department of Mechanic Engineering & Engineering Science, National University of Singapore, Singapore 117575, Singapore;* orcid.org/0000-0001-6198-5753; Email: shenlei@nus.edu.sg

Authors

Yang Li − *School of Materials and Energy, Southwest University, Chongqing 400715, China*

Junhan Wu − *School of Materials and Energy, Southwest University, Chongqing 400715, China*

Chunmei Li − *School of Materials and Energy, Southwest University, Chongqing 400715, China;* orcid.org/0000-0002-8822-7036

Complete contact information is available at: https://pubs.acs.org/10.1021/acsomega.1c00840

Author Contributions

‖Y.L. and J.W. contributed equally to this work.

Notes

The authors declare no competing financial interest.

The data that support the findings of this study can be obtained from the corresponding author upon reasonable request.

■ ACKNOWLEDGMENTS

This work was financially supported by the Sumin Zeng Project in Southwest University (ZSM2021008), the Fundamental Research Funds for the Central Universities (XDJK2017B043), and the Singapore MOE Tier 1 grant (R- 265-000-691-114).

■ REFERENCES

(1) Krätschmer, W.; Lamb Lowell, D.; Fostiropoulos, K.; Huffman Donald, R. Solid C60: a new form of carbon. *Nature* **1990**, *347*, 354−358.

(2) Iijima, S. Helical microtubules of graphitic carbon. *Nature* **1991**, *354*, 56−58.

(3) Novoselov, K. S.; Geim, A. K.; Morozov, S. V.; Jiang, D.; Zhang, Y.; Dubonos, S. V.; Grigorieva, I. V.; Firsov, A. A. Electric Field Effect in Atomically Thin Carbon Films. *Science* **2004**, *36*, 666−669.

(4) Baughman, R. H.; Eckhardt, H.; Kertesz, M. Structure-property predictions for new planar forms of carbon: Layered phases containing Sp2 and sp atoms. *J. Chem. Phys.* **1987**, *87*, 6687−6699.

(5) Li, Y.; Xu, L.; Liu, H.; Li, Y. Graphdiyne and graphyne: from theoretical predictions to practical construction. *Chem. Soc. Rev.* **2014**, *43*, 2572.
(6) Peng, Q.; Dearden, A. K.; Crean, J.; Han, L.; Liu, S.; Wen, X.; De, S. New materials graphyne, graphdiyne, graphone, and graphane: review of properties, synthesis, and application in nanotechnology. *Nanotechnol., Sci. Appl.* **2014**, *7*, 1−29.
(7) Li, G. X.; Li, Y. L.; Liu, H. B.; Guo, Y. B.; Li, Y. J.; Zhu, D. B. Architecture of graphdiyne nanoscale films. *Chem. Commun.* **2010**, *46*, 3256−3258.
(8) Shang, H.; Zou, Z.; Li, L.; Wang, F.; Liu, H. B.; Li, Y. J.; Li, Y. L. Ultrathin Graphdiyne Nanosheets Grown In Situ on Copper Nanowires and Their Performance as Lithium-Ion Battery Anodes. *Angew. Chem., Int. Ed.* **2018**, *57*, 774−778.
(9) Zhou, W. X.; Shen, H.; Wu, C.; Tu, Z.; He, F.; Gu, Y.; Xue, Y.; Zhao, Y.; Yi, Y.; Li, Y.; Li, Y. Direct Synthesis of Crystalline Graphdiyne Analogue Based on Supramolecular Interactions. *J. Am. Chem. Soc.* **2019**, *141*, 48−52.
(10) Han, Y. Y.; Lu, X. L.; Tang, S. F.; Yin, X. P.; Wei, Z. W.; Lu, T. B. Metal-Free 2D/2D Heterojunction of Graphitic Carbon Nitride/Graphdiyne for Improving the Hole Mobility of Graphitic Carbon Nitride. *Adv. Energy Mater.* **2018**, *8*, 1702992−1702999.
(11) He, J.; Bao, K.; Cui, W.; Yu, J.; Huang, C.; Shen, X.; Cui, Z.; Wang, N. Construction of Large-Area Uniform Graphdiyne Film for High-Performance Lithium-Ion Batteries. *Chem. - Eur. J.* **2018**, *24*, 1187−1192.
(12) Liu, R.; Liu, H.; Li, Y.; Yi, Y.; Shang, X.; Zhang, S.; Yu, X.; Zhang, S.; Cao, H.; Zhang, G. Nitrogen-doped graphdiyne as a metal-free catalyst for high-performance oxygen reduction reactions. *Nanoscale* **2014**, *6*, 11336−11343.
(13) Liu, R.; Zhou, J.; Gao, X.; Li, J.; Xie, Z.; Li, Z.; Zhang, S.; Tong, L.; Zhang, J.; Liu, Z. Graphdiyne Filter for Decontaminating Lead-Ion-Polluted Water. *Adv. Electron. Mater.* **2017**, *3*, No. 1700122.
(14) Parvin, N.; Jin, Q.; Wei, Y.; Yu, R.; Zheng, B.; Huang, L.; Zhang, Y.; Wang, L.; Zhang, H.; Gao, M.; et al. Few-Layer Graphdiyne Nanosheets Applied for Multiplexed Real-Time DNA Detection. *Adv. Mater.* **2017**, *29*, No. 1606755.
(15) Wang, S.; Yi, L.; Halpert, J. E.; Lai, X.; Liu, Y.; Cao, H.; Yu, R.; Wang, D.; Li, Y. A Novel and Highly Efficient Photocatalyst Based on P25−Graphdiyne Nanocomposite. *Small* **2012**, *8*, 265−271.
(16) Xue, Y.; Zou, Z.; Li, Y.; Liu, H.; Li, Y. Graphdiyne-Supported NiCo2S4 Nanowires: A Highly Active and Stable 3D Bifunctional Electrode Material. *Small* **2017**, *13*, No. 1700936.
(17) Zhang, H.; Xia, Y.; Bu, H.; Wang, X.; Zhang, M.; Lou, Y.; Zhao, M. Graphdiyne: A promising anode material for lithium ion batteries with high capacity and rate capability. *J. Appl. Phys.* **2013**, *113*, No. 044309.
(18) Zhang, S.; Liu, H.; Huang, C.; Cui, G.; Li, Y. Bulk graphdiyne powder applied for highly efficient lithium storage. *Chem. Commun.* **2015**, *51*, 1834−1837.
(19) Zou, Z.; Shang, H.; Chen, Y.; Li, J.; Liu, H.; Li, Y.; Li, Y. A facile approach for graphdiyne preparation under atmosphere for an advanced battery anode. *Chem. Commun.* **2017**, *53*, 8074−8077.
(20) Padilha, J. E.; Fazzio, A.; Silva, A. J. R. Directional Control of the Electronic and Transport Properties of Graphynes. *J. Phys. Chem. C* **2014**, *118*, 18793−18798.
(21) Chen, J.; Xi, J.; Wang, D.; Shuai, Z. Carrier Mobility in Graphyne Should Be Even Larger than That in Graphene: A Theoretical Prediction. *J. Phys. Chem. Lett.* **2013**, *4*, 1443−1448.
(22) Kuang, C.; Tang, G.; Jiu, T.; Yang, H.; Liu, H.; Li, B.; Luo, W.; Luo, W.; Li, X.; Zhang, W.; Lu, F.; et al. Highly Efficient Electron Transport Obtained by Doping PCBM with Graphdiyne in Planar-Heterojunction Perovskite Solar Cells. *Nano Lett.* **2015**, *15*, 2756−2762.
(23) Luo, G.; Qian, X.; Liu, H.; Qin, R.; Zhou, J.; Li, L.; Gao, Z.; Wang, E.; Mei, W. N.; Lu, J.; et al. Quasiparticle energies and excitonic effects of the two-dimensional carbon allotrope graphdiyne: Theory and experiment. *Phys. Rev. B: Condens. Matter Mater. Phys.* **2011**, *84*, No. 075439.
(24) Perdew, J. P.; Burke, K.; Ernzerhof, M. Generalized Gradient Approximation Made Simple. *Phys. Rev. Lett.* **1997**, *78*, 1396.
(25) Segall, M. D.; Lindan, P. J. D.; Probert, M.; Pickard, C. J.; Hasnip, P. J.; Clark, S. J.; Payne, M. C. First-principles simulation: ideas, illustrations and the CASTEP code. *J. Phys.: Condens. Matter* **2002**, *14*, 2717.
(26) Vanderbilt, D. Soft self-consistent pseudopotentials in a generalized eigenvalue formalism. *Phys. Rev. B: Condens. Matter Mater. Phys.* **1990**, *41*, 7892.
(27) Grimme, S.; Antony, J.; Ehrlich, S.; Krieg, H. A consistent and accurate ab initio parametrization of density functional dispersion correction (DFT-D) for the 94 elements H-Pu. *J. Chem. Phys.* **2010**, *132*, No. 154104.
(28) Chadi, D. J. Special points for Brillouin-zone integrations. *Phys. Rev. B: Condens. Matter Mater. Phys.* **1977**, *16*, 1746.
(29) Puigdollers, A. R.; Alonso, G.; Gamallo, P. First-principles study of structural, elastic and electronic properties of α-, β- and γ-graphyne. *Carbon* **2016**, *96*, 879−887.
(30) Dickman, S.; Senozan, N. M.; Hunt, R. L. Thermodynamic Properties and the Cohesive Energy of Calcium Ammoniate. *J. Chem. Phys.* **1970**, *52*, 2657−2663.
(31) Ducéré, J.-M.; Lepetit, C.; Chauvin, R. Carbo-graphite: Structural, Mechanical, and Electronic Properties. *J. Phys. Chem. C* **2013**, *117*, 21671−21681.
(32) Naritta, N.; Nagai, S.; Suzuki, S.; Nakao, K. Optimized geometries and electronic structures of graphyne and its family. *Phys. Rev. B* **1998**, *58*, 11009.
(33) Yue, Q.; Chang, S.; Kang, J.; Qin, S.; Li, J. Mechanical and Electronic Properties of Graphyne and Its Family under Elastic Strain: Theoretical Predictions. *J. Phys. Chem. C* **2013**, *117*, 14804−14811.
(34) Cranford, S. W.; Brommer, D. B.; Buehler, M. Extended graphynes: simple scaling laws for stiffness, strength and fracture. *Nanoscale* **2012**, *4*, 7797−7809.
(35) Harald, I.; Hans, L.; Laszlo, M.; David, M. Solid-State Physics: An Introduction to Theory and Experiment. *Am. J. Phys.* **1992**, *60*, 1053−1054.
(36) Srinivasu, K.; Ghosh, S. K. Graphyne and Graphdiyne: Promising Materials for Nanoelectronics and Energy Storage Applications. *J. Phys. Chem. C* **2012**, *116*, 5951−5956.
(37) Zhou, J.; Lv, K.; Wang, Q.; Chen, X. S.; Sun, Q.; Jena, P. Electronic structures and bonding of graphyne sheet and its BN analog. *J. Chem. Phys.* **2011**, *134*, No. 174701.
(38) Long, M.; Tang, L.; Wang, D.; Li, Y.; Shuai, Z. Electronic Structure and Carrier Mobility in Graphdiyne Sheet and Nanoribbons: Theoretical Predictions. *ACS Nano* **2011**, *5*, 2593−2600.
(39) Zheng, Q.; Luo, G.; Liu, Q.; Quhe, R.; Zheng, J.; Tang, K.; Gao, Z.; Nagase, S.; Lu, J. Structural and electronic properties of bilayer and trilayer graphdiyne. *Nanoscale* **2012**, *4*, 3990−3996.
(40) Shen, L.; Zeng, M.; Yang, S. W.; Zhang, C.; Wang, X.; Feng, Y. Electron Transport Properties of Atomic Carbon Nanowires between Graphene Electrodes. *J. Am. Chem. Soc.* **2010**, *132*, 11481−11486.
(41) Zhang, L.; Li, H.; Feng, Y. P.; Shen, L. Diverse Transport Behaviors in Cyclo[18]carbon-Based Molecular Devices. *J. Phys. Chem. Lett.* **2020**, *11*, 2611−2617.
(42) Tran, F.; Blaha, P. Importance of the Kinetic Energy Density for Band Gap Calculations in Solids with Density Functional Theory. *J. Phys. Chem. A* **2017**, *121*, 3318−3325.
(43) Deák, P.; Aradi, B.; Frauenheim, T.; Janzén, E.; Gali, A. Accurate defect levels obtained from the HSE06 range-separated hybrid functional. *Phys. Rev. B* **2010**, *81*, No. 153203.
(44) Kang, J.; Li, J.; Wu, F.; Li, S. S.; Xia, J. B. Elastic, Electronic, and Optical Properties of Two-Dimensional Graphyne Sheet. *J. Phys. Chem. C* **2011**, *115*, 20466−20470.
(45) Okoye, C. M. I. Theoretical study of the electronic structure, chemical bonding and optical properties of KNbO3 in the paraelectric cubic phase. *J. Phys.: Condens. Matter* **2003**, *15*, 5945.
(46) Kronig, R. D. L. On the Theory of Dispersion of X-Rays. *J. Opt. Soc. Am.* **1926**, *12*, 547−557.

https://doi.org/10.1021/acsomega.1c00840
ACS Omega 2021, 6, 10997−11004

(47) Xie, Z.; Hui, L.; Wang, J.; Zhu, G.; Chen, Z.; Li, C. Electronic and optical properties of monolayer black phosphorus induced by bi-axial strain. *Comput. Mater. Sci.* **2018**, *144*, 304−314.
(48) Zheng, S.; Wu, E.; Feng, Z.; Zhang, R.; Xie, Yuan.; Yu, Y.; Zhang, R.; Li, Q.; Liu, J.; Pang, W.; et al. Acoustically enhanced photodetection by a black phosphorus−MoS2 van der Waals heterojunction p−n diode. *Nanoscale* **2018**, *10*, 10148−10153.
(49) Almeida, J. S.; Ahuja, R. Tuning the structural, electronic, and optical properties of BexZn1−xTe alloys. *Appl. Phys. Lett.* **2006**, *89*, No. 061913.
(50) Ma, T. H.; Yang, C. H.; Xie, Y.; Sun, L.; Lv, W. Q.; Wang, R.; Zhu, C. Q.; Wang, M. Electronic and optical properties of orthorhombic LiInS2 and LiInSe2: A density functional theory investigation. *Comput. Mater. Sci.* **2009**, *47*, 99−105.
(51) Srikant, V.; Clarke, D. R. Optical absorption edge of ZnO thin films: The effect of substrate. *J. Appl. Phys.* **1997**, *81*, 6357.

https://doi.org/10.1021/acsomega.1c00840
ACS Omega 2021, 6, 10997−11004